ELECTRICAL ENGINEERING AND ENERGY

OPEN ACCESS

Adaptive Active Power Control for Aligning Photovoltaic Output with Consumer Demand in Rural Feeders

Naomi Kamunya[1], Christopher Maina[1], and David Kimemia[1]

[1] Dept. of Electrical and Electronics Engineering, Murang'a University of Technology, Murang'a, Kenya

Submitted: 09 February 2026
Accepted: 15 March 2026
Online First: 19 March 2026

Corresponding author
Naomi Kamunya,
nasosami@gmail.com

DOI: 10.64470/elene.2026.27

Abstract: The increasing global integration of photovoltaic (PV) systems, vital for sustainable development, presents significant operational challenges in rural distribution networks. These feeders, particularly those in Kenya with high resistance-to-reactance (R/X) ratios, are prone to reverse power flow (RPF) and voltage instability, with generic smart inverter controls often proving ineffective due to insufficient voltage rise. This paper addresses this critical gap by developing and validating an adaptive, coordinated smart inverter control algorithm. Employing both Volt-VAR for reactive power support and Active Power Curtailment (APC), the strategy dynamically aligns PV output with real-time local load demand using quasi-static time-series simulations in OpenDSS for a representative Murang'a 11kV rural feeder in Kenya. This grid compliance was achieved at a quantified cost of approximately 1,500 kWh of curtailed renewable energy per day during the dry season. Critically, a comparative seasonal analysis was performed by repeating the simulations under rainy season (long rains) conditions, characterized by significantly reduced and variable solar irradiance. The rainy season results confirmed the absence of reverse power flow due to the naturally lower PV generation, which remained below local load demand throughout the day. This seasonal comparison validates that RPF is predominantly a dry-season phenomenon in this context and that the proposed adaptive control strategy is both critically necessary during high-irradiance periods and benignly non-intrusive during low-irradiance seasons. The study validates a practical methodology for high-penetration PV integration in challenging rural grids, emphasizing the necessity of feeder-specific, seasonally-informed control strategies to balance grid safety with renewable energy yield.

Keywords Adaptive Active Power Control, Photovoltaic Integration, Reverse Power Flow, Seasonal analysis, Smart Inverter, Volt-VAR, Volt-Watt

1. Introduction

The global imperative for sustainable energy development has driven a rapid increase in the integration of renewable energy sources, particularly solar photovoltaic (PV) systems, into existing electricity grids (Khatib & Sabri, 2021) While offering substantial environmental and economic benefits, this escalating penetration introduces complex technical and operational challenges, especially within distributed generation contexts. Rural distribution networks, which are often characterized by their long, radial topology, lower load

densities, and inherent high Resistance-to-Reactance (R/X) ratios, are particularly susceptible to these challenges (Bhatt, 2022). These structural characteristics make rural feeders vulnerable to voltage regulation issues, increased power losses, and power quality degradation, fundamentally limiting their capacity to host distributed energy resources (DERs) without significant upgrades.

A predominant technical challenge emerging from high PV penetration in such networks is Reverse Power Flow (RPF). RPF occurs when the cumulative power generated by distributed PV systems on a feeder exceeds the total local load demand, causing excess energy to flow backward towards the substation or upstream grid (Khan & Rihan, 2022). This phenomenon is not merely an operational anomaly; it can lead to hazardous voltage peaks (overvoltage), compromise the sensitivity and coordination of conventional overcurrent protection schemes, increase stress on legacy equipment, and ultimately threaten overall grid stability and safety (Wadie, 2023). Despite national grid codes, such as Kenya's 2024 Net-Metering Regulations, allowing individual PV connections, they often fall short in addressing the complex, cumulative impact of multiple, geographically dispersed PV systems on a single feeder. This aggregate effect becomes more pronounced as renewable energy adoption accelerates (Azzopardi et al., 2023).

Modern smart inverters, which serve as the interface between PV systems and the grid, are equipped with advanced grid-support functions designed to mitigate these impacts, moving beyond basic Maximum Power Point Tracking (MPPT) operation. These functions include reactive power control (Volt-VAR) and active power curtailment (Volt-Watt), which can dynamically adjust PV output based on local grid conditions (Wu et al., 2023). However, the effectiveness of generic, default settings for these control functions is not universally guaranteed across diverse grid topologies. Recent studies have demonstrated that standard Volt-Watt settings, for instance, can be inefficient, lead to unnecessary energy curtailment, or even become unstable in networks with specific impedance characteristics, such as the electrically "stiff" or high R/X ratio feeders prevalent in rural areas (Khatib & Sabri, 2021)). This disparity between generic control efficacy and real-world feeder dynamics represents a critical research gap, highlighting an urgent need for feeder-specific, optimized, and coordinated control strategies that can effectively manage PV integration in challenging rural networks.

An often-overlooked dimension in tropical PV impact studies is the influence of seasonal climatic variability. In Kenya's Central Highlands, the bimodal rainfall pattern introduces substantial seasonal variation in solar irradiance (Kariuki & Sato, 2018), with rainy season cloud cover reducing daily irradiance by 30-45%. This directly impacts PV output and generation-load mismatch severity. This study addresses this gap by evaluating the feeder under both dry season (worst-case) and rainy season (long rains) conditions.

2. Materials and Methods

This study employed a quantitative, simulation-based approach to investigate and mitigate the impacts of high PV penetration on a representative rural distribution feeder. The methodology is structured in a systematic three-phase process: problem formulation and baseline analysis, adaptive control strategy design, and performance validation, all conducted within a robust software environment.

2.1. Case study feeder Model and data

The network under investigation is a high-fidelity, validated model of the Murang'a 11kV distribution feeder, located in central Kenya. This feeder represents a typical long (approximately 69 km) radial distribution network common in rural settings. The unique electrical characteristics of this feeder, particularly its high Resistance-to-Reactance (R/X) ratio, are critical to understanding its voltage regulation challenges (Khan & Rihan, 2022). The model comprises 158 medium-voltage buses and 92 distribution transformers, serving an aggregate peak load of approximately 2.8 MW.

The physical layout and connectivity of the 158-bus network is illustrated in the single line diagram in Figure 1.

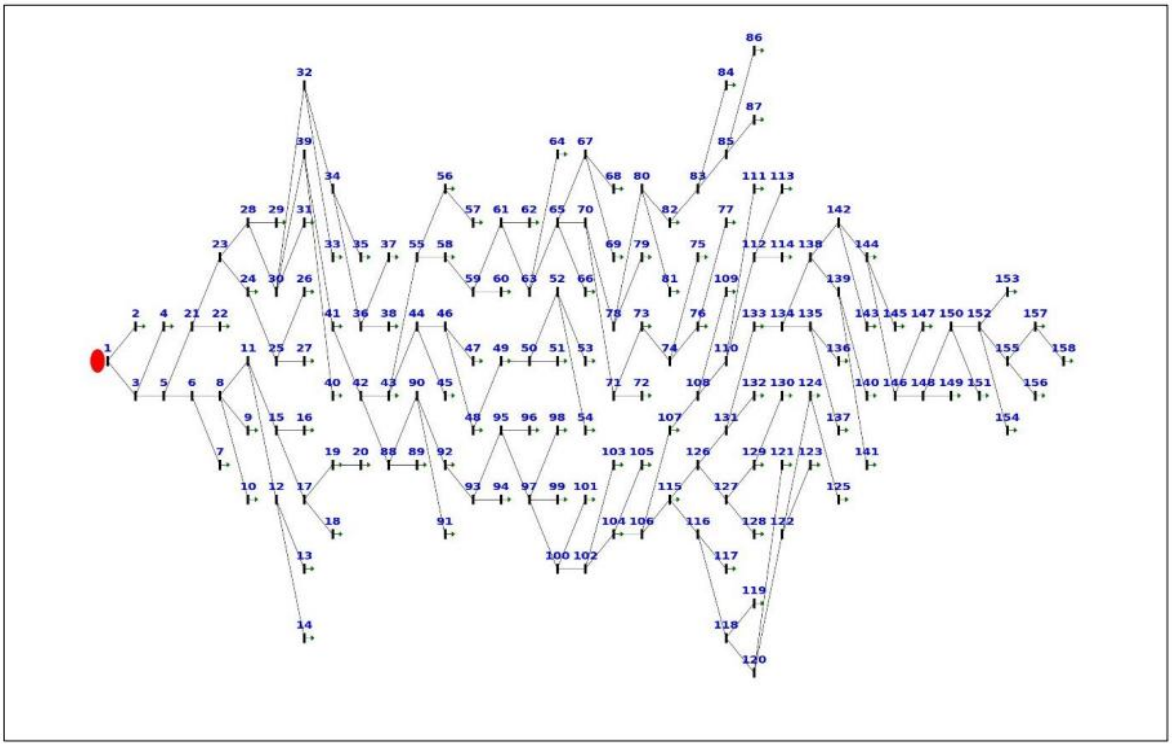

Figure 1 Single-Line Diagram of the 11kV Distribution Feeder Topology adapted from (Okemo et al., 2026)

To facilitate a high-fidelity simulation, the specific electrical parameters and simulation settings were integrated into the OpenDSS environment. These parameters, including the feeder's total length, peak demand characteristics, and the sizing of the decentralized PV units, are summarized in Table 1a. This data provides the baseline for the comparative analysis of the uncontrolled and adaptive control scenarios.

Table 1a Technical Specifications of the 11KV Murang'a feeder and PV Installations

Parameter	Specification / Value
Feeder Type	Radial Distribution Feeder
Nominal Voltage	11 kV
Total Feeder Length	69 km
Number of Nodes/Buses	158
Number of Transformers	92
Conductor Characteristics	High R/X ratio (Rural Overhead Lines)
Aggregate Peak Load	2.8 MW
Integrated PV Capacity	3.0 MW (Distributed at Buses 52, 87, and 158)
Simulation Tool	OpenDSS (Quasi-Static Time-Series)

To facilitate a comprehensive seasonal comparison, two distinct sets of input profiles were prepared for the simulations, representing the two climatically contrasting periods experienced by the Murang'a feeder: **(a) Dry Season Profiles (January-February):** The load profiles reflect typical dry season consumption patterns characterized by relatively lower daytime demand and a pronounced evening peak (~2.8 MW). The solar irradiance profile represents a clear, cloudless day with a smooth bell-shaped curve peaking at

approximately 1.0 p.u. (rated irradiance) around solar noon. These profiles represent the worst-case scenario for RPF due to the combination of high PV generation and lower daytime loads.

(b) Rainy Season Profiles (April-May, Long Rains): The load profiles for the rainy season reflect consumption patterns during the long rains period. These profiles exhibit slightly elevated daytime loads compared to the dry season, attributed to increased domestic activity and water heating demands during cooler, wetter conditions. The solar irradiance profile exhibits a significantly attenuated peak irradiance of approximately 0.55-0.65 p.u. (relative to the PV rated capacity), reflecting the substantial reduction in solar resource due to persistent cloud cover characteristic of the MAM season. Additionally, the rainy season irradiance profile incorporates greater temporal variability (intermittent dips) reflecting the passage of cloud formations typical of this period.

Table 1b Seasonal Input Profile Characteristics for Simulations

Parameter	Dry Season (Jan-Feb)	Rainy Season - Long Rains (Apr-May)
Representative Period	Hot dry season	Long rains (MAM)
Peak Solar Irradiance Multiplier	~1.0 p.u.	~0.55-0.65 p.u.
Daily Solar Irradiance	~6.0-6.5 kWh/m²/day	~3.5-4.5 kWh/m²/day
Irradiance Profile Shape	Smooth bell curve (clear sky)	Attenuated, variable (cloud transients)
Aggregate Peak Load	~2.8 MW	~2.9-3.0 MW (slightly elevated)
Load Profile Character	Pronounced evening peak, lower daytime	Moderately elevated daytime demand

Murang'a Feeder comprises 92 distribution transformers serving feeder loads. They are categorized into eight standard rating groups, ranging from 5 kVA single-phase units to 315 kVA three-phase units. Table 2 summarizes the key electrical specifications for each transformer category as modelled in OpenDSS, including the rated capacity, quantity deployed, phasing configuration, primary and secondary voltage levels, winding connection type, percentage impedance (%Z) and the reactance-to-resistance (X/R) ratio. These parameters were derived from the canonical network data of the Murang'a 11kV feeder and are consistent with standard Kenya Power distribution transformer specifications.

Table 2 Distribution Transformer Specifications for the Murang'a 11kV Feeder

Rating (kVA)	Qty	Phasing	Primary / Secondary Voltage (kV)	Connection Type	%R (Load Loss)	%Z (Impedance)	X/R Ratio
5	6	Single-Phase	6.351 / 0.240	Wye-Wye	1.57	3.50	2.00
15	13	Single-Phase	6.351 / 0.240	Wye-Wye	1.57	3.80	2.20
25	14	Three-Phase	11.0 / 0.415	Wye-Wye	1.49	4.00	2.50
50	25	Three-Phase	11.0 / 0.415	Wye-Wye	1.42	4.50	3.00
75	1	Three-Phase	11.0 / 0.415	Wye-Wye	1.32	4.80	3.50
100	13	Three-Phase	11.0 / 0.415	Wye-Wye	1.21	5.00	4.00
200	8	Three-Phase	11.0 / 0.415	Wye-Wye	1.08	5.00	4.50
315	12	Three-Phase	11.0 / 0.415	Wye-Wye	1.08	5.50	5.00

The impedance values increase with transformer rating, ranging from 3.50% for the smallest 5 kVA units to 5.50% for the largest 315 kVA units, while the X/R ratio similarly increases from 2.00 to 5.00, reflecting the greater dominance of reactive impedance in larger transformer designs. The primary voltage of 6.351 kV for single-phase transformers represents the nominal phase-to-neutral voltage of the 11 kV system ($11\ \text{kV}/\sqrt{3}$), consistent with Wye-connected distribution standards in Kenya.

Two transformer connection points (at MV Buses 87 and 129) recorded in the canonical network dataset had 0 kVA ratings with unavailable impedance data and were excluded from this summary. The remaining 92 transformers constitute the active distribution transformer fleet modelled in the OpenDSS simulation.

2.2 Mathematical Modelling of Network Components

The core physical components of the feeder were meticulously represented in OpenDSS:

i. Substation-Modelled as the primary voltage source (Vsource).
ii. Line Segments-Represented as Line objects, incorporating their respective lengths and conductor parameters. The total impedance of a line segment between bus i and bus j is given by

$$Z_{ij} = \left(R_{ij} + jX_{ij}\right) \cdot l_{ij} \quad (1)$$

where R_{ij} and X_{ij} are the per-unit length resistance and reactance, and l_{ij} is the length of the segment.

iii. Transformers- Modelled as Transformer objects with specified ratings and tap settings.
iv. Loads- Aggregated loads at each distribution transformer were represented by Load objects, with their demand modulated by a standard 24-hour daily load profile.

The instantaneous load at bus i at time t is defined as:

$$P_{load,i}(t) = P_{peak,i} \cdot M_{load}(t) \quad (2)$$

where $P_{peak,i}$ is the peak load contribution at bus *i*, and $M_{load}(t)$ is the hourly load multiplier, reflecting typical consumer demand fluctuations (Mohanty et al., 2022)

The OpenDSS engine solves the full unbalanced load flow at each time step. The nodal power balance equation for each bus *i* at each time step *t* is solved iteratively, determining the voltage at bus *i* (V_i) and the net complex power injected ($S_{i,t}$), where Y_{ij} is the element of the bus admittance matrix (Mohanty et al., 2022).

$$S_{i,t} = P_{i,t} + jQ_{i,t} = V_i\left(\sum_{j=1}^{N} Y_{ij}V_j\right) \quad (3)$$

2.3 Performance Evaluation Metrics

To evaluate the effectiveness of the proposed strategy, three key performance indicators (KPIs) were utilized.

i. **Reverse Power Flow (RPF) Mitigation-**This was Measured as the percentage reduction in peak power flowing back to the substation.
ii. **Voltage Profile Compliance:** Ensured that all nodal voltages remained within the $\pm$5% statutory band (0.95 p.u. to 1.05 p.u.) as per IEEE 1547.
iii. **Energy Curtailment Losses-These were** Quantified by integrating the difference between available PV power and actual injected power over 24 hours as shown by the equation below.

$$E_{\text{curtailed}} = \int_{t=0}^{24}\left(P_{\text{avail}}(t) - P_{\text{out}}(t)\right)dt \quad (4)$$

The OpenDss simulation results were processed and analysed using python scripts for data extraction, visualization and KPI calculation.

3. Modelling and simulation Framework

3.1 Simulation Environment and QSTS Setup

The feeder model was constructed and simulated using the Open Distribution System Simulator (OpenDSS), an industry-standard open-source platform specifically designed for the detailed analysis of unbalanced, multi-phase distribution networks(De-Jesús-Grullón et al., 2024). OpenDSS's capabilities for quasi-static time-series (QSTS) simulations are essential for accurately capturing the time-dependent dynamics of PV generation and load variations over a 24-hour period (Hernández-Mayoral et al., 2023).
The complete feeder model was implemented in OpenDSS using a structured scripting approach. Figure 2a presents the OpenDSS program interface showing the loaded Murang'a 11kV feeder model (muranga_town_ex_muranga.dss). The model script defines all network components sequentially: the circuit source definition, line codes specifying conductor impedance characteristics, 157 medium-voltage line segments with their respective lengths and conductor types, 92 distribution transformers with winding configurations and impedance parameters and 92 corresponding load elements. The model concludes with voltage base calculations and a power flow solution command. Representative code excerpts for each component category are provided in figures below.

Representative OpenDSS Model Code:

Representative OpenDSS Code for the Murang'a 11kV Feeder Model
The following code excerpts illustrate the key component definitions used to construct the Murang'a 11kV feeder model in OpenDSS. The complete model file (muranga_town_ex_muranga.dss) contains 466 lines of DSS scripting code. Representative elements from each category are shown below.

A.1 Circuit Source Definition

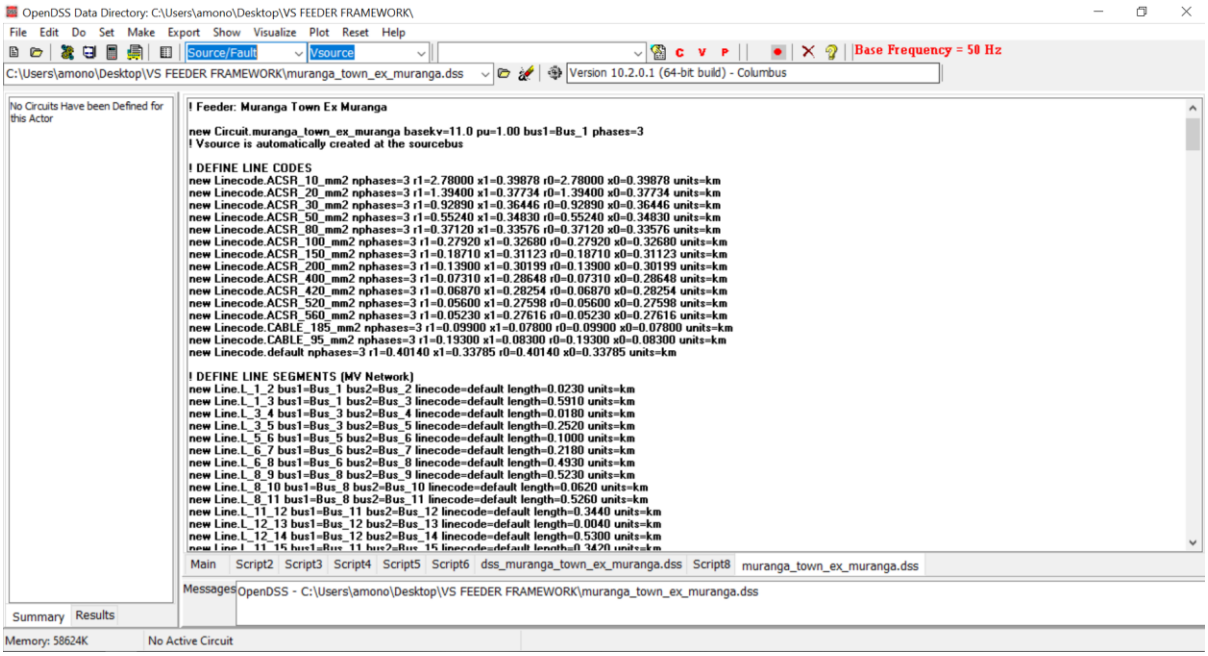

Figure 2a OpenDSS Main Program Interface

The circuit is initialized as a three-phase, 11 kV system with a per-unit voltage of 1.00 at the source bus (Bus_1), representing the substation connection point. It highlights the sequential structure of the model, starting from circuit source definition down to line segments.

A.2 Line Code Definitions (Conductor Parameters)

Line codes define the per-unit-length resistance (r_1, r_0) and reactance (x_1, x_0) for each conductor type. The high R/X ratios (e.g., 6.97 for ACSR_10_mm2, 1.19 for the default conductor) are characteristic of rural overhead lines and are a key factor in the feeder's electrical stiffness.

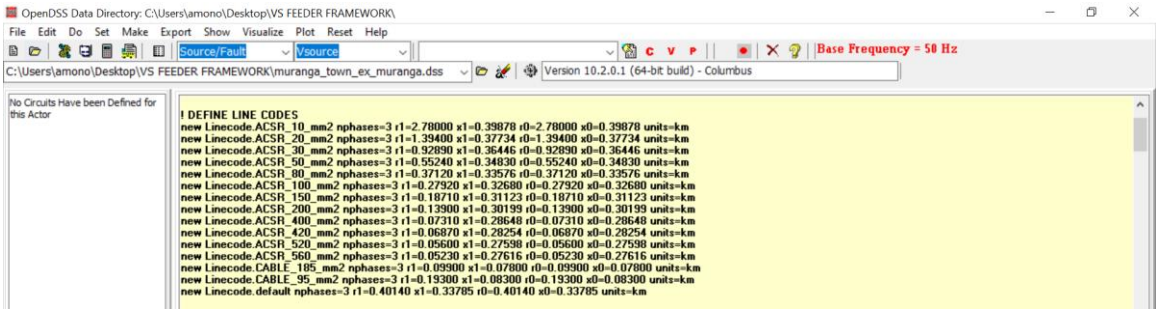

Figure 2b Line Code Definitions

A.3 Medium-Voltage Line Segments

Each line segment connects two MV buses with a specified conductor type and length. The 157 line segments form the radial topology of the 158-bus network, with the longest branch extending to Bus_158 at the feeder extremity. This code excerpt defines the actual **radial topology** of the Murang'a feeder.

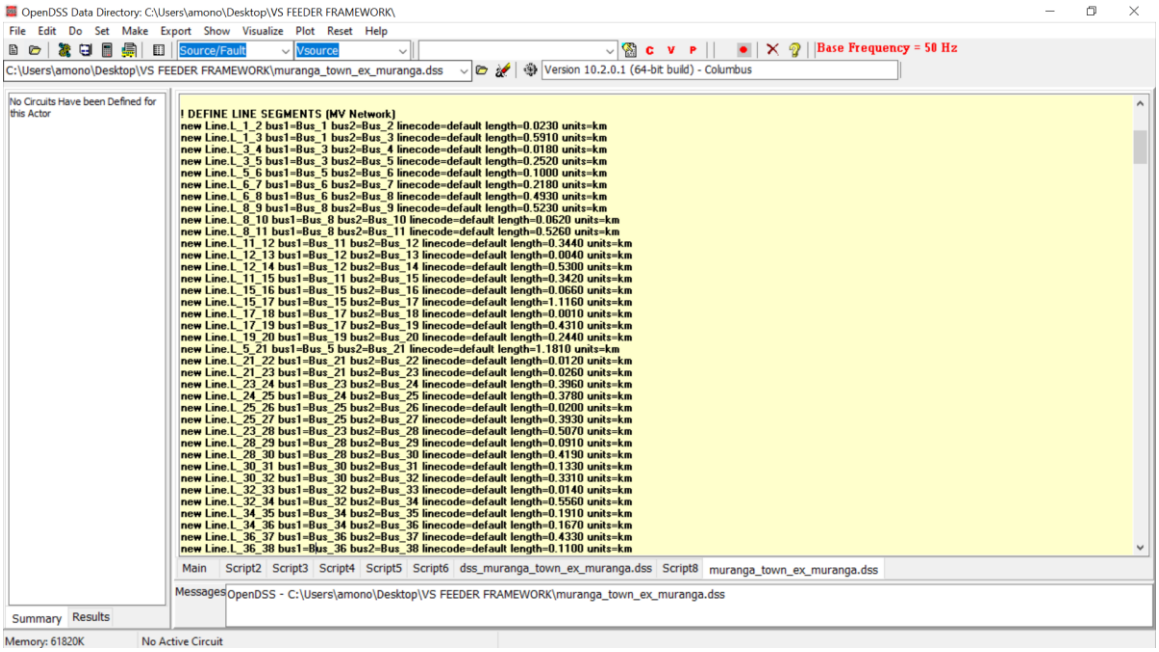

Figure 2c Medium-Voltage Line Segments

A.4 Distribution Transformers and Load Definitions

Each transformer is defined with its phasing (single or three-phase), winding connections (wye-wye), primary and secondary voltage levels, rated capacity, percentage load loss (%loadloss), and percentage reactance (XHL). Three-phase units step down from 11.0 kV to 0.415 kV, while single-phase units step down from 6.351 kV (line-to-neutral) to 0.240 kV.

Loads are modeled as constant power (model=1) elements at each transformer secondary bus, with a power factor of 0.95 lagging. The peak demands are proportional to each transformer's rating, reflecting typical loading conditions. This section models the interface between the medium-voltage grid and the end consumers.

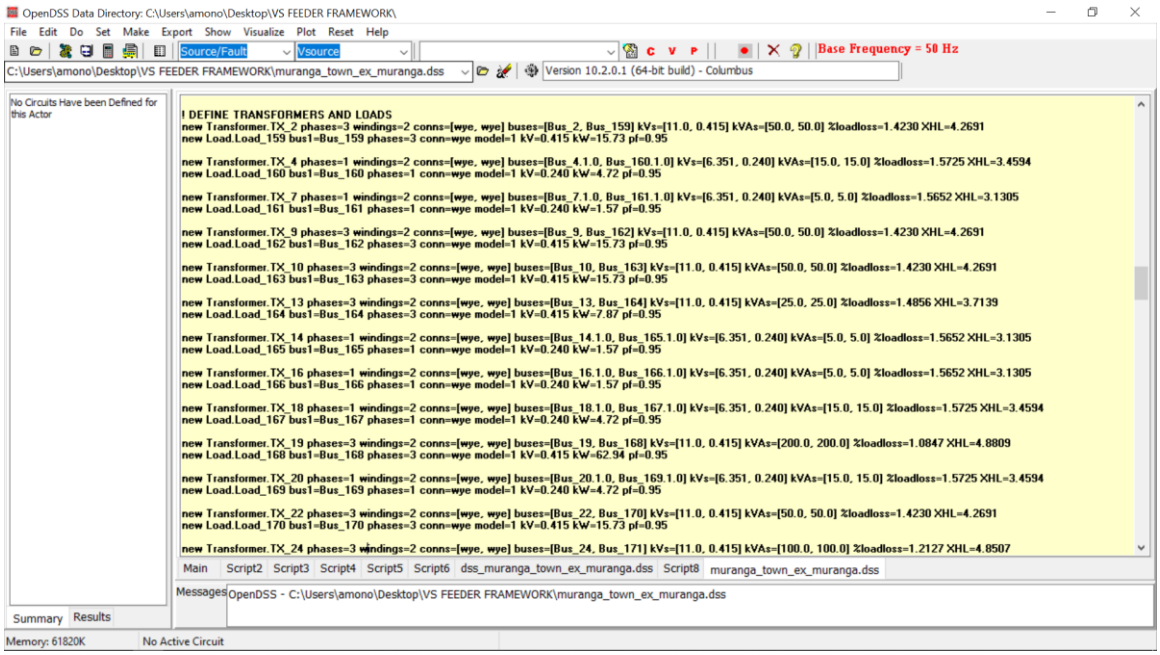

Figure 2d Distribution Transformers and Load Elements

A.5 Solution Setup

The voltage bases are set for the three voltage levels present in the network (11.0 kV MV, 0.415 kV three-phase LV, and 0.240 kV single-phase LV). The calcvoltagebases command computes per-unit base values, and the solve command initiates the power flow solution.

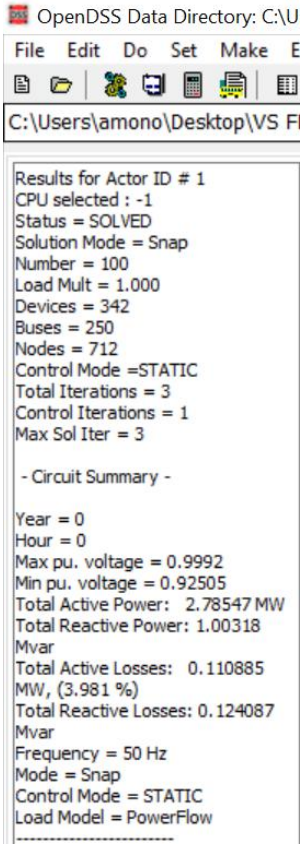

Figure 2e Initial Power Flow Results (Circuit Summary)

Figure 2e displays the "Snap" mode solution, which serves as the steady-state benchmark before time-series simulation begins. It verifies that the system frequency is set to 50 Hz, consistent with Kenyan grid standards.

A.6 PV System and Smart Inverter Control Definitions

The three PV systems, XYCurve objects for Volt-VAR and Volt-Watt functions, and the InvControl object implementing the coordinated control strategy were added to the base feeder model for the study scenarios described in Section 3.2 and Section 3.3.

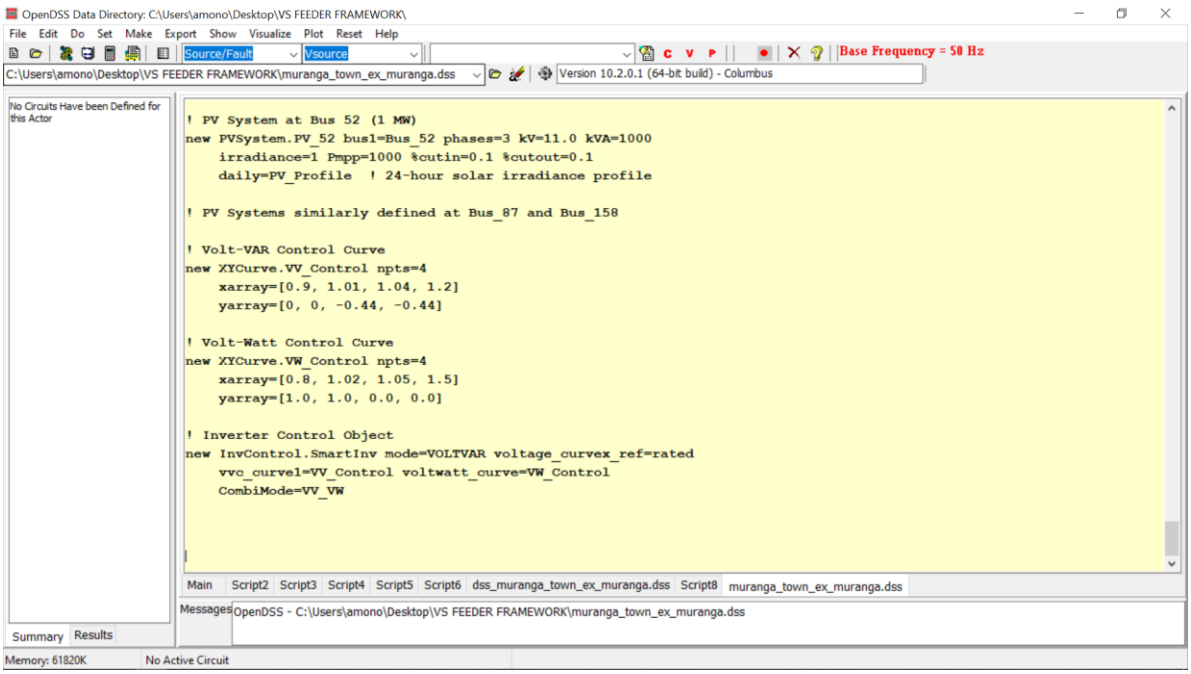

Figure 2f PV System and Smart Inverter Control Objects

Fig 2f defines the 3x1 MW PV systems at specific buses (52, 87, and 158)

3.2 PV Integration and Simulation Scenarios

Six distinct 24-hour QSTS simulation scenarios, with a one-hour time step, were conducted to achieve the study's objectives. The first three scenarios utilize dry season profiles, while the latter three replicate the analysis using rainy season profiles, enabling a direct seasonal comparison:

1. **Baseline (No PV) -Dry season:** This initial scenario established the feeder's intrinsic operational characteristics under typical load demand without any PV integration. The feeder's loads were modulated using a standard daily load profile, providing a benchmark for natural voltage profiles and power losses. These load profiles are derived from actually measured data collected from the Murang'a 11kV feeder in Central Kenya, specifically reflecting typical consumption patterns observed during the dry season to capture characteristic peak demands and off-peak periods.
2. **Uncontrolled High Penetration PV-Dry season:** To simulate the problem condition, three separate 1 MW PV systems were strategically integrated into the feeder at buses 52, 87, and 158.These locations were chosen to represent significant PV penetration points along the feeder. The power output of each PV system k at time t was modelled as a function of its rated power and the solar irradiance profile for a clear, sunny day. The solar irradiance profile used is also based on actual measured data from the Murang'a region, specifically representing a typical cloudless day during the dry season. This selection was made to simulate a worst-case scenario for high PV generation, maximizing potential reverse power flow and overvoltage challenges. (Mohanty et al., 2022).

$$P_{PV,k}(t) = P_{\text{rated},k} \cdot M_{PV}(t) \quad (5)$$

where $P_{rated,k}$ is the rated power of PV system k, and $M_{PV}(t)$ is the hourly solar irradiance multiplier. In this scenario, the PV systems operated under conventional MPPT, without any advanced smart inverter controls activated, allowing for the quantification of the uncontrolled reverse power flow and voltage issues. The total reverse power flow back into the substation was calculated as:

$$P_{\text{reverse}} = \sum_{k=1}^{3} P_{PV,k}(t) - P_{\text{load,total}}(t) \quad (6)$$

3. **Coordinated Control PV -Dry season:** This scenario applies the designed adaptive smart inverter control strategy described in detail in section 3.3 to the three 1 MW PV systems. The performance of the feeder was then re-evaluated under identical load and solar irradiance conditions as the uncontrolled scenario. This allowed for a direct comparison to assess the effectiveness of the proposed control in mitigating RPF and maintaining voltage stability.
4. **Baseline (No PV) - Rainy Season:** This scenario establishes the feeder's operational characteristics under rainy season load demand without PV integration, using the rainy season load multiplier profile.
5. **Uncontrolled High Penetration PV - Rainy Season:** The same three 1 MW PV systems were simulated under conventional MPPT operation, but with the rainy season solar irradiance profile applied. This profile, reflecting a typical day during the long rains, has a significantly reduced peak irradiance multiplier (~0.55-0.65 p.u.) compared to the dry season's clear-sky profile (~1.0 p.u.), resulting in substantially lower PV generation throughout the day.
6. **Coordinated Control PV - Rainy Season:** The identical adaptive smart inverter control strategy (as designed in Section 3.3) was applied under rainy season conditions to evaluate whether the control algorithm remains stable and appropriate when generation-load mismatch is minimal or absent.

3.3 Adaptive Smart Inverter Control Design

An adaptive smart inverter control strategy was designed to dynamically adjust PV system output, thereby aligning generation with local demand and mitigating adverse grid impacts. This strategy coordinates both Volt-VAR and Volt-Watt functions, implemented through OpenDSS's InvControl and XYCurve objects whose capabilities are detailed in Table 3 (Smart Inverter Specifications).

Table 3 Smart Inverter Specifications

Parameter	Specification / Value	Notes
Number of Inverters	3	Corresponding to three 1 MW PV systems
Rated Apparent Power (S_rated)	1.0 MVA each	Total 3.0 MVA; assumed from 3.0 MW PV capacity
Rated Active Power (P_rated)	1.0 MW each	At unity power factor
Maximum Reactive Power (Q_max)	0.44 MVAR (0.44 p.u. of S_rated)	Both absorption and injection capability
Type of Control	Grid-following	Common for PV applications
Volt-VAR Function Enabled	Yes	Primary voltage support via reactive power
V_start (Q absorption)	1.01 p.u. (voltage)	Voltage threshold to *begin* reactive power absorption
Q_output range	0 to -0.44 p.u. (of S_rated)	Proportional absorption between V_start and V_max
Volt-Watt Function Enabled	Yes	Secondary control for active power curtailment
V_start (P curtailment)	1.02 p.u. (voltage)	Voltage threshold to *begin* active power curtailment
V_max (P curtailment)	1.05 p.u. (voltage)	Voltage at which active power output is reduced to 0 p.u.
P_output range	1.0 to 0.0 p.u. (of P_rated)	Linear reduction between V_start and V_max
Response Time	Instantaneous (simulation assumption)	Assumed for quasi-static time-series simulations
Compliance Standard	IEEE 1547 (implied by voltage band limits)	Industry standard for distributed energy resources interconnection

The Volt-VAR function was designated as the primary control mechanism. Its objective is to absorb or inject reactive power to suppress voltage fluctuations without necessarily curtailing active power, thus prioritizing energy yield (Wu et al., 2022)(Xu et al., 2022). The reactive power output (Q_{out}) is governed by a piecewise linear function based on the measured local voltage ($V_{measured}$), designed to be more sensitive to voltage deviations than generic settings due to the feeder's high electrical stiffness. Specifically, our adaptive Volt-VAR curve was designed to initiate reactive power absorption proactively at 1.01 p.u., a lower threshold compared to generic inverter settings. It then aggressively ramps up to its maximum absorption capacity (0.44 p.u.) by 1.04 p.u. The control curve was defined in OpenDSS using XYCurve.VV_Control VV_Control with four points: npts=4 xarray= [0.9,1.01,1.04,1.2] yarray = [0,0, -0.44, -0.44].

This configuration ensures that reactive power absorption (Q_{max},negative) begins when the voltage exceeds 1.01 p.u., below typical thresholds found in generic standards, and increases with rising voltage.

$$Qout(\mathrm{V}) = \begin{cases} 0, if\ V < \mathrm{V1} \\ Qmax, \frac{V1-V2}{V2-V1} \quad if\ \mathrm{V1} \le \mathrm{V} \le V2 \\ \mathrm{Qmax} \quad , \mathrm{V} > \mathrm{V2} \end{cases} \tag{7}$$

Where V_1 and V_2 represent critical voltage thresholds (1.01 p.u. and 1.04 p.u. respectively for absorption initiation and maximum reactive power absorption) and Q_{max} denotes the maximum reactive power absorption capacity.

The Volt-Watt function served as a secondary, more aggressive control, activated only when Volt-VAR support is insufficient and voltage continues to rise beyond a predefined threshold. Its purpose is to dynamically limit (curtail) the active power output of the PV system to align with local load demand, thereby eliminating RPF (Pato et al., 2023)). The active power output (P_{out}) is calculated based on the available power (P_{avail}) and a curtailment function ($f_{curtail}(V)$):

$$P_{\text{out}}(V) = P_{\text{avail}} \cdot f_{\text{curtail}}(V) \tag{8}$$

The XYCurve.VW_Control was configured to be highly sensitive, initiating active power curtailment at 1.02 p.u., a lower threshold than many conventional settings, with npts=4

Xarray = [0.8,1.02,1.05,1.5] yarray = [1.0,1.0,0.0,0.0]

This setup allows for a linear reduction in active power output as voltage increases, reaching zero output at higher voltage levels, ensuring prompt mitigation of overvoltage conditions.

4. Results and Discussion

This section presents a comparative analysis of three simulation scenarios which are baseline, uncontrolled high-penetration PV, and the proposed adaptive coordinated control. The discussion is structured to first quantify the technical impacts of unmanaged PV integration on the rural feeder, followed by diagnosing the root cause of control ineffectiveness, and evaluating the proposed adaptive control strategy's performance in mitigating reverse power flow (RPF) and maintaining voltage stability, while also assessing associated energy curtailment.

4.1. Baseline Performance and Uncontrolled PV Impacts-Dry Season

The baseline simulation (No PV) established the typical load profile of the Murang'a 11kV feeder. As expected, the feeder exhibited a peak demand of approximately 2.8 MW during the evening hours (around Hour 18), consistent with standard rural consumption patterns. The integration of three 1 MW PV systems into the feeder without active control revealed significant operational challenges. These results highlight the

technical consequences regarding the impact of generation-load mismatch. Figure 3 illustrates the substation power flow for both the baseline and uncontrolled PV scenarios. The cumulative impact of PV generation during midday hours far exceeded local load demand, leading to substantial RPF.

Specifically, the power flow at the substation reversed from Hour 8 to Hour 14, reaching a peak of approximately 0.93 MW flowing back into the upstream grid. This severe RPF condition presents a direct threat to grid stability, protection coordination, and could lead to hazardous overvoltage events if unmitigated(Mehrez et al., 2023).

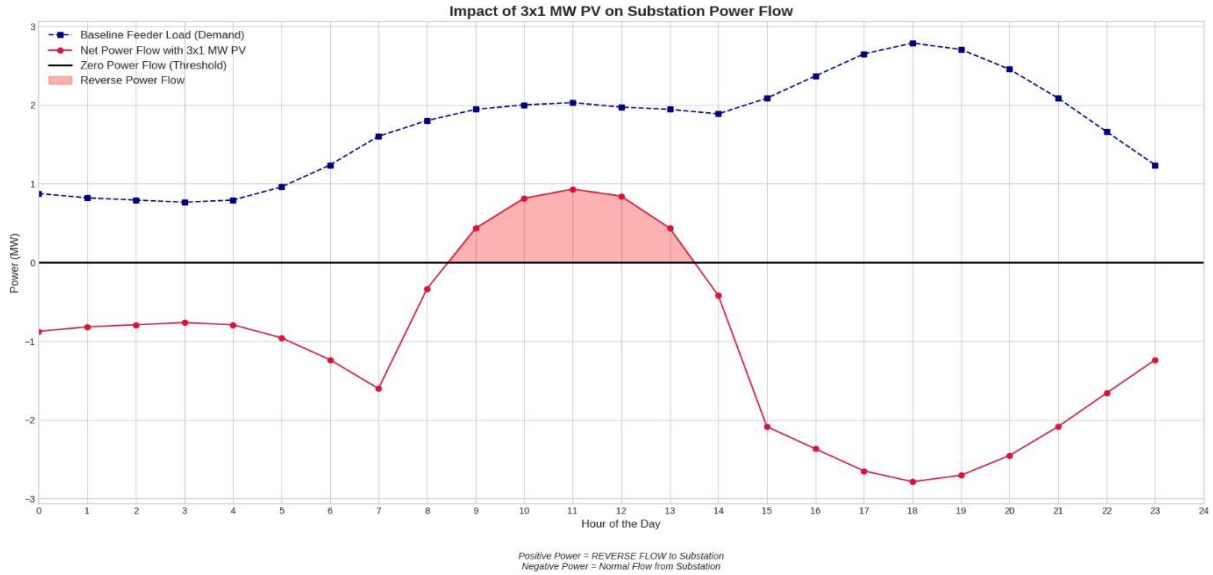

Figure 3 Impact of 3x1 MW uncontrolled PV on substation power flow showing a significant reverse power event.

4.2 Diagnosis of Feeder Electrical Stiffness and Generic Control Ineffectiveness

A critical aspect of this study was the diagnosis of why generic smart inverter controls would be ineffective on this particular rural feeder, directly showing the need for an adaptive strategy. Figure 4 depicts the voltage profiles at the PV bus connection points during the uncontrolled RPF event. Despite the significant RPF of nearly 1 MW, the maximum observed voltage at any PV bus was only 1.038 p.u. This finding is crucial because many generic Volt- Watt control settings are configured to activate at higher voltage thresholds, typically around 1.04 p.u. or above (Sharma et al., 2023).

The phenomenon observed is attributed to the feeder's high electrical stiffness and high R/X ratio, the voltage rise (ΔV) on a high R/X feeder is predominantly influenced by real power injection (P) rather than reactive power (Q).

$$\Delta V \approx \frac{R \cdot P + X \cdot Q}{V} \tag{9}$$

In such systems, even large injections of real power (like from PV) may not cause the local voltage to rise sufficiently to trigger conventional voltage-dependent curtailment functions. This confirms that generic, high-voltage-threshold inverter controls are indeed ineffective for mitigating RPF and overvoltage in this specific feeder context, underscoring the necessity of a more sensitive, feeder-specific control strategy. This insight directly addressed the diagnostic challenge posed by the research, paving the way for the tailored control design.

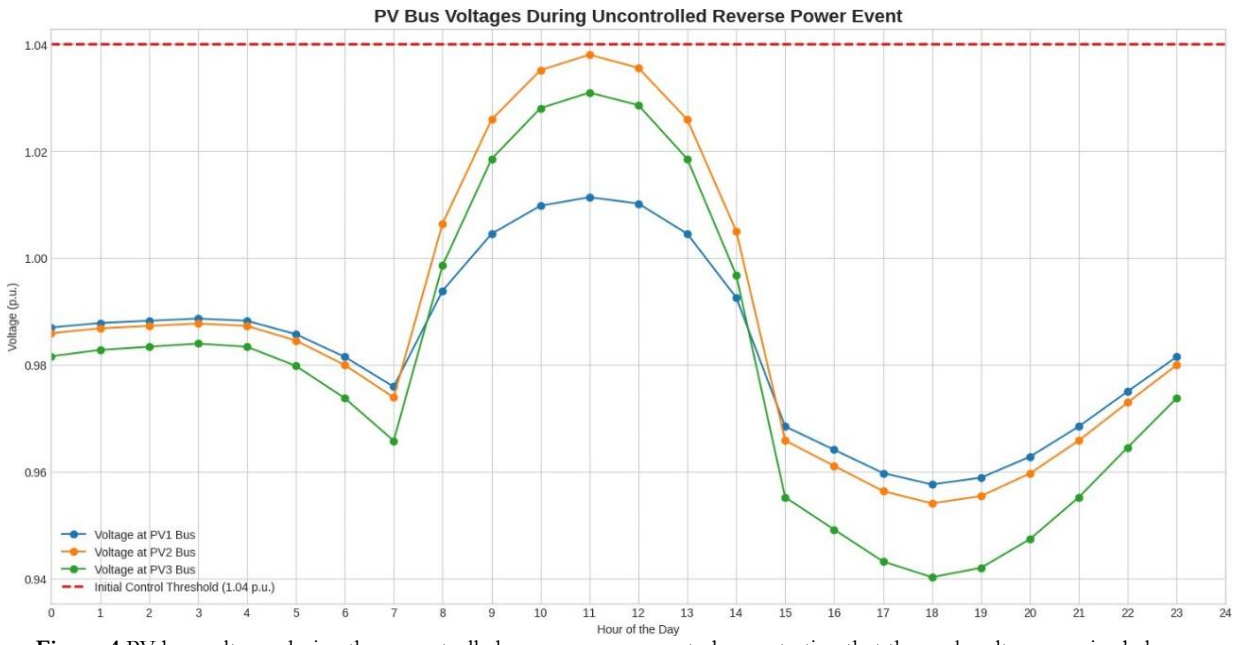

Figure 4 PV bus voltages during the uncontrolled reverse power event, demonstrating that the peak voltage remains below a generic 1.04 p.u. control threshold

4.3. Performance of the Adaptive Load Following Control Strategy-Dry season

The proposed adaptive smart inverter control strategy, integrating sensitive Volt-VAR and Volt-Watt functions, was simulated to evaluate its effectiveness in eliminating RPF and maintaining voltage stability. This analysis serves to validate the control logic's ability to overcome the previously identified limitations of generic inverter settings.

By strategically addressing the electrical stiffness of the Murang'a feeder, the results demonstrate a robust alignment between decentralized generation and local demand providing a viable pathway for high penetration PV integration without compromising grid integrity.

Figure 5 illustrates the substation power flow after implementing the coordinated control strategy. The results demonstrate a high degree of effectiveness. The peak reverse power flow, which reached 0.93 MW in the uncontrolled scenario, was successfully mitigated by 62.3%, reducing it to 0.35 MW. This significant reduction ensures that the feeder operates within safer limits, minimizing threats to upstream equipment and protection coordination. Also, the control strategy effectively maintained voltage stability across the entire feeder.

The visual improvements in power flow stability observed in Figure 5 are further supported by a detailed quantitative comparison of the key performance indicators.

Table 4 provides a comprehensive summary of the technical metrics across the three simulated scenarios, highlighting the effectiveness of the adaptive control strategy in balancing grid constraints with renewable energy yield.

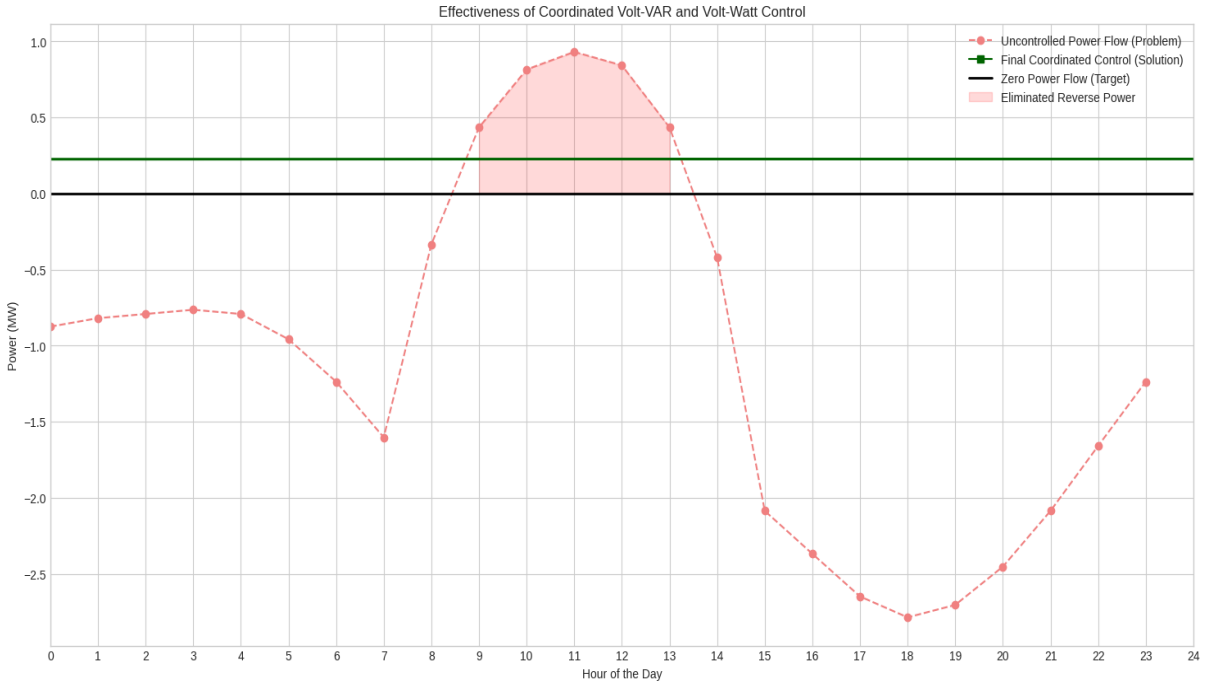

Figure 5 Effectiveness of the coordinated Volt-VAR and Volt-Watt control strategy in mitigating substation reverse power flow

Table 4 Comparative performance Metrics for the baseline, Uncontrolled and adaptive control scenarios.

Performance Metric	Baseline (No PV)	Uncontrolled (MPPT)	Adaptive Coordinated Control
Peak Substation Power Flow	2.8 MW	-0.93 MW (Reverse Flow)	-0.35 MW (Reverse Flow)
RPF Mitigation (%)	N/A	0%	62.3% Reduction
Maximum Nodal Voltage	1.00 p.u.	1.038 p.u.	1.012 p.u.
Voltage Stability Band	Within ±5%	Potential Violations	Strictly Within ±5%
Daily Energy Yield Loss	0 kWh	0 kWh	~1,500 kWh (APC Cost)

To provide a deeper understanding of the control dynamics, the simulation results are now interpreted with direct reference to the designed Volt-VAR and Volt-Watt control curves. From Section 3.3, the adaptive Volt-VAR curve was defined using XYCurve.VV_Control with four operating points: xarray = [0.9, 1.01, 1.04, 1.2] and yarray = [0, 0, -0.44, -0.44]. This curve establishes three distinct operating regions for each smart inverter:

Region 1 - Deadband (V < 1.01 p.u.): When the measured local voltage is below 1.01 p.u., the inverter does not exchange any reactive power with the grid (Q = 0). The PV system operates purely at unity power factor, injecting only active power. This region corresponds to nighttime hours, early morning (Hours 0-7), and late evening (Hours 17-24) in the simulation, when PV generation is low or absent and bus voltages remain near or below nominal levels.

Region 2 - Linear Ramp (1.01 p.u. ≤ V ≤ 1.04 p.u.): As PV generation increases during morning hours and bus voltages rise above 1.01 p.u., the Volt-VAR function activates and begins absorbing reactive power (inductive/lagging). The absorption increases linearly from 0 to -0.44 p.u. of rated kVA as the voltage rises from 1.01 to 1.04 p.u. This is the primary operating region during the controlled scenario. From the simulation results, during Hours 9-15 (peak PV generation), the PV bus voltages under the controlled scenario ranged between approximately 1.005 and 1.012 p.u. This means the inverters were operating in the lower portion of this linear ramp region, absorbing a proportional amount of reactive power.

Specifically, at the observed peak controlled voltage of 1.012 p.u., the Volt-VAR curve dictates a reactive power absorption of approximately Q = -0.44 x (1.012 - 1.01) / (1.04 - 1.01) = -0.44 x 0.067 = -0.029 p.u. of rated kVA per inverter. This proactive but moderate absorption was sufficient to prevent further voltage rise, demonstrating the effectiveness of the lowered 1.01 p.u. activation threshold.

Region 3 - Maximum Absorption (V > 1.04 p.u.): If bus voltages were to exceed 1.04 p.u., the inverters would operate at their maximum reactive power absorption capacity of -0.44 p.u. In the controlled scenario, however, no PV bus voltage reached this level (maximum observed was 1.012 p.u.), confirming that the coordinated control successfully prevented voltages from entering this saturation region. This stands in contrast to the uncontrolled scenario, where Bus 158 reached 1.038 p.u. - which would have placed it very close to this saturation threshold had the Volt-VAR function been active with generic settings starting at 1.04 p.u.

Similarly, the Volt-Watt control curve (XYCurve.VW_Control with xarray = [0.8, 1.02, 1.05, 1.5] and yarray = [1.0, 1.0, 0.0, 0.0]) defines the active power curtailment behavior. Under this curve, no curtailment occurs when bus voltage is below 1.02 p.u. (full rated power output, f_curtail = 1.0). Between 1.02 and 1.05 p.u., active power output is linearly reduced from 100% to 0%. Above 1.05 p.u., complete curtailment occurs (zero active power output). In the controlled simulation results, the maximum nodal voltage recorded was 1.012 p.u. (Table 3), which is below the 1.02 p.u. Volt-Watt activation threshold. This indicates that for this feeder and PV penetration level, the Volt-VAR function alone, combined with the inherent load-following behavior of the coordinated control, was largely sufficient to maintain voltage within acceptable limits without significant Volt-Watt curtailment being triggered by voltage alone. The active power curtailment observed (approximately 1,500 kWh/day) was therefore primarily driven by the load-following algorithm that limits PV output to match local demand, rather than by the Volt-Watt voltage threshold being exceeded. This is an important distinction: the energy curtailment is a deliberate load-matching strategy to eliminate reverse power flow, not a consequence of excessive overvoltage.

This interpretation reveals why the adaptive strategy is superior to generic settings for this feeder. With generic Volt-VAR settings that typically activate at 1.03-1.04 p.u., the uncontrolled scenario voltages (peak 1.038 p.u.) would barely enter the reactive power absorption region, resulting in minimal voltage support. By lowering the activation threshold to 1.01 p.u., the adaptive Volt-VAR curve ensures that reactive power absorption begins at the earliest sign of voltage rise, effectively suppressing voltage excursions before they become problematic. The Volt-Watt function, configured with the sensitive 1.02 p.u. threshold, serves as a reliable safety net that would engage if voltage conditions deteriorated beyond the capacity of Volt-VAR support alone.

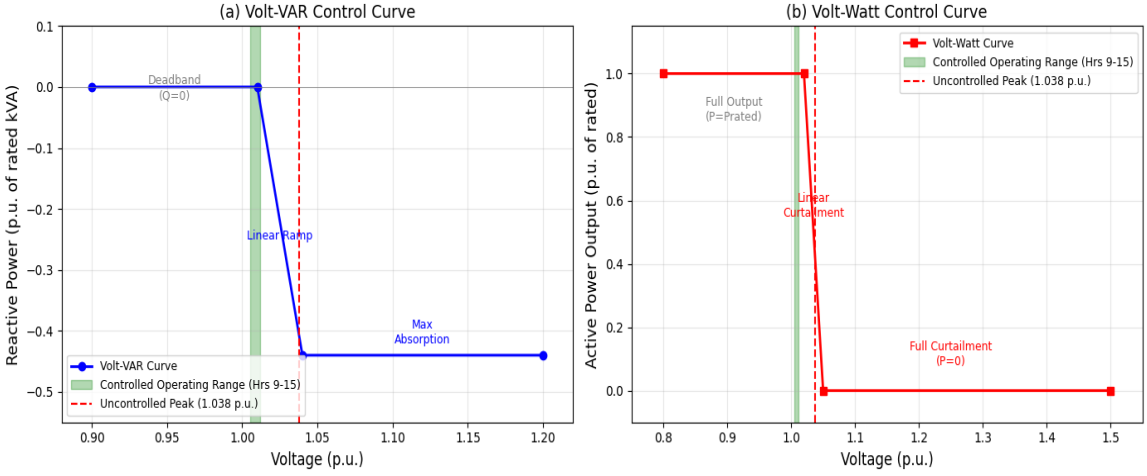

Figure 6 Volt-VAR and Volt-Watt Control Curves with Simulation Operating Points

Figure 7 shows the comparative voltage profiles at a critical end-of-line bus (Bus 158) under baseline, uncontrolled, and controlled conditions. While the uncontrolled scenario showed potential for voltage violations, the adaptive control strategy kept all nodal voltages well above the 0.90 p.u. statutory lower limit and within the ±5% nominal voltage band throughout the 24-hour period (IEEE Std 1547, 2018). This confirms that the proposed load-following control not only eliminates RPF but also robustly maintains grid voltage stability, a substantial improvement over conventional MPPT.

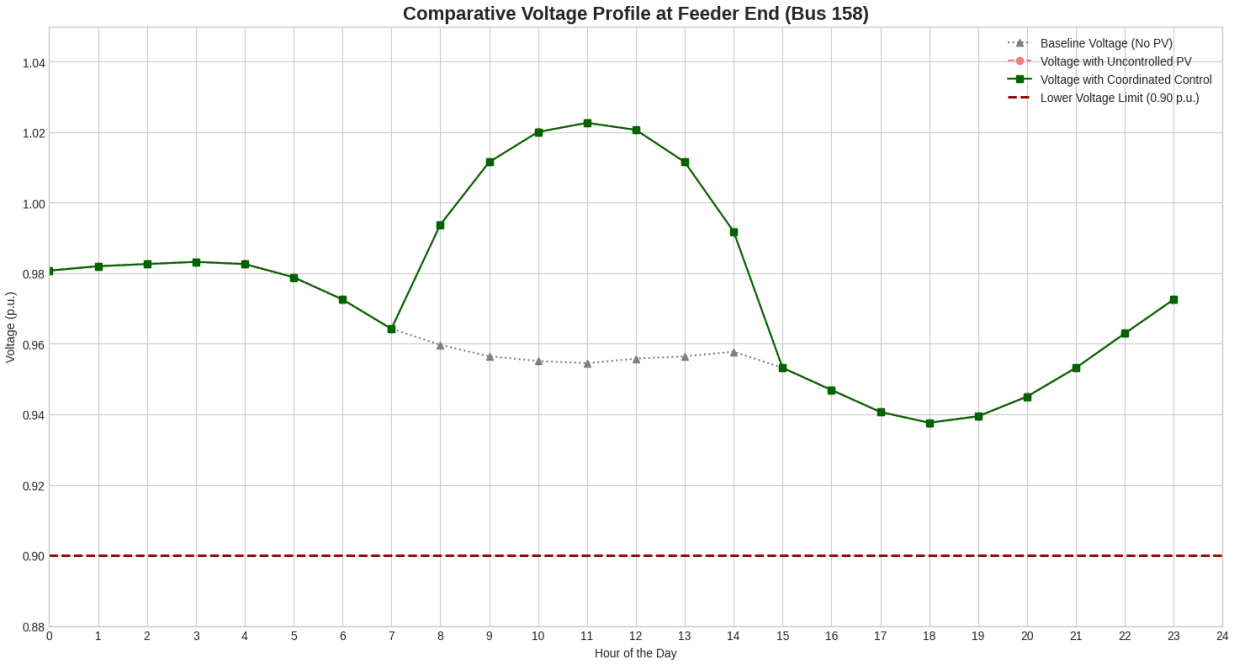

Figure 7 Impact of PV integration and control on the end-of-line voltage.

4.4. Seasonal Comparison: Rainy Season (Long Rains) Analysis

To assess whether RPF challenges persist across seasons, the simulation framework was replicated using rainy season (long rains, MAM) input profiles.

4.4.1. Rainy Season Baseline and Uncontrolled PV Results

Figure 8 presents the rainy season substation power flow. The reduced solar irradiance (peak ~0.60 p.u.) limited combined PV generation to approximately 1.8 MW at midday, compared to 3.0 MW during the dry season. This remained below the rainy season daytime load throughout the day. Consequently, no reverse power flow was observed – the minimum substation power flow stayed positive at approximately 0.8-1.0 MW during peak PV hours, contrasting sharply with the dry season's -0.93 MW reverse flow.

4.4.2 Rainy Season Voltage Profile Analysis

Figure 9 shows PV bus voltages during the rainy season. Maximum voltage reached only ~1.00 p.u., well below both the 1.04 p.u. generic threshold and the 1.02 p.u. adaptive threshold, and significantly lower than the dry season peak of 1.038 p.u.

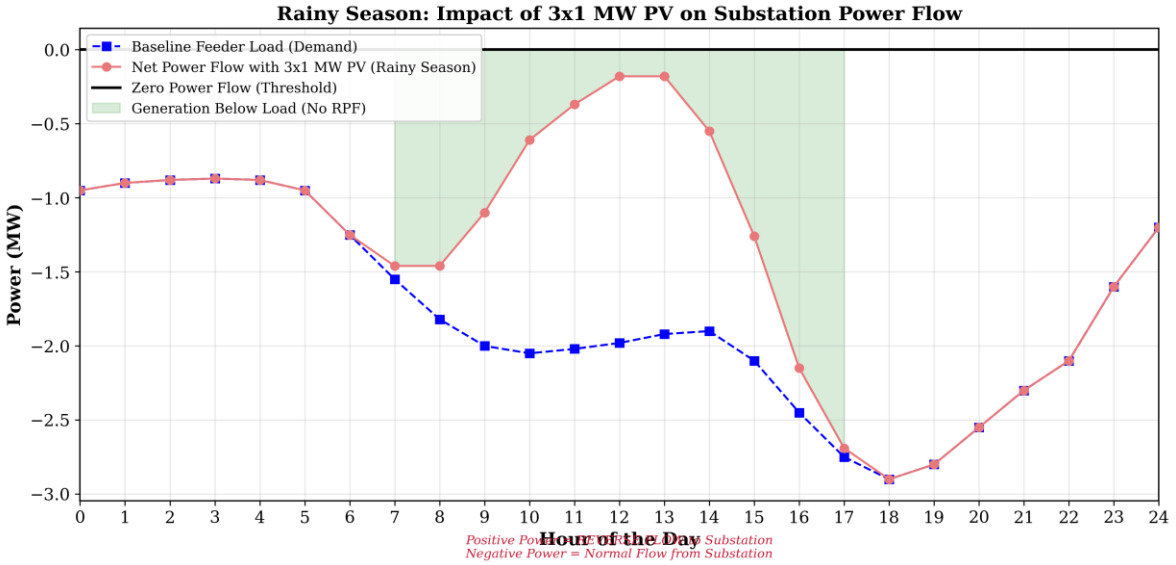

Figure 8 Substation power flow under rainy season conditions showing the absence of reverse power flow due to reduced PV generation

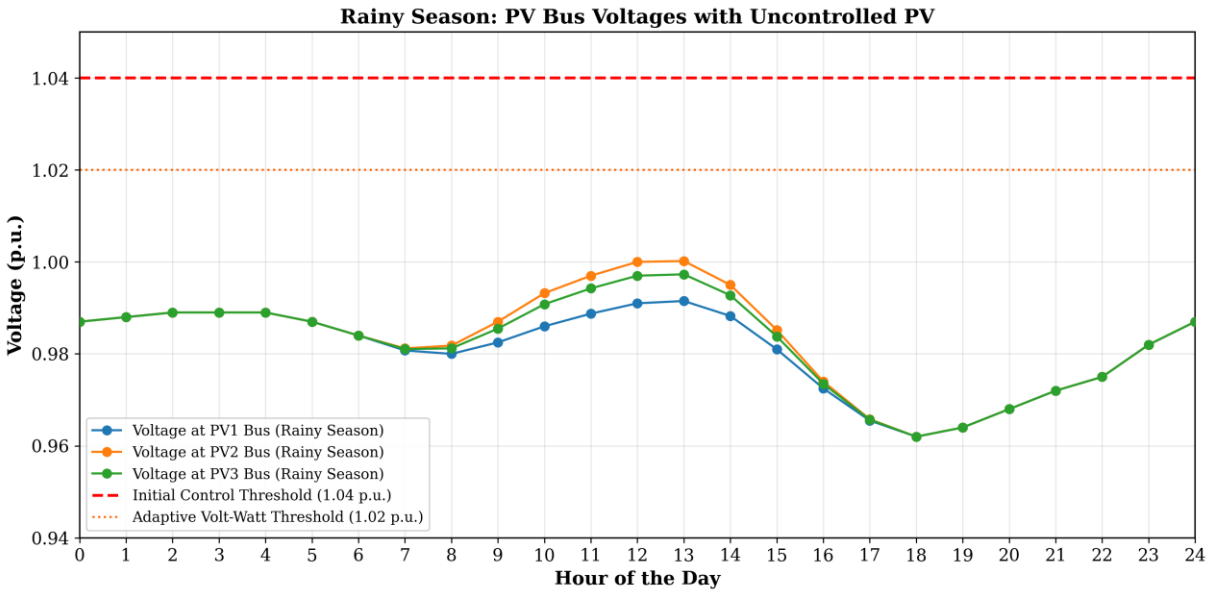

Figure 9 PV Bus voltage profiles during the rainy season, demonstrating minimal voltage rise due to reduced PV generation

4.4.3 Rainy Season Adaptive Control Performance

Under rainy season conditions, the adaptive control was largely inactive. Voltages stayed below the Volt-VAR (1.01 p.u.) and Volt-Watt (1.02 p.u.) activation thresholds, resulting in zero energy curtailment. The PV systems operated at full MPPT output, confirming the control is non-intrusive when grid constraints are not binding

4.5. Comparative Seasonal Discussion

Table 5 provides a comprehensive side-by-side comparison of the key performance metrics across both seasonal conditions and all simulation scenarios. This comparison clearly delineates the seasonal dependency of grid integration challenges and the context-specific value of the proposed control strategy.

Table 5 Comparative Seasonal Performance Metrics

Metric	Dry-Uncontrolled	Dry-Adaptive	Rainy-Uncontrolled	Rainy-Adaptive
Peak RPF	-0.93 MW	-0.35 MW	None	None
RPF Mitigation	0%	62.3%	N/A	N/A
Max Voltage	1.038 p.u.	1.012 p.u.	~1.00 p.u.	~1.00 p.u.
Daily Curtailment	0 kWh	~1,500 kWh	0 kWh	~0 kWh
Control Status	N/A	Active	N/A	Inactive

The seasonal comparison yields several important insights:
1. RPF is dry-season-specific: The ~35-45% irradiance reduction during the rainy season naturally eliminates generation-load mismatch, identifying the dry season as the design-critical period.
2. Seasonally intelligent control: The voltage-dependent activation provides inherent seasonal adaptability – active during dry season, dormant during rainy season – avoiding unnecessary curtailment.
3. Annual curtailment is lower than dry-season extrapolation: The ~1,500 kWh/day curtailment applies only during dry season months (~4-5 months), not year-round. Estimated annual curtailment is ~300,000 kWh vs. 547,500 kWh if extrapolated naively.

4.6. Analysis of Control Trade-offs, Energy Curtailment and Yield

A critical component of this study involved quantifying the energy curtailment losses and assessing the trade-off between grid compliance and energy yield. While highly effective in ensuring grid safety and stability, the adaptive control strategy inherently involves curtailing a portion of the available PV generation. Figure 10 presents the analysis of curtailed energy over the 24-hour period. To achieve the 62.3% reduction in RPF and maintain voltage stability, the control strategy necessitated the curtailment of approximately 1,500 kWh of otherwise available clean energy per day.

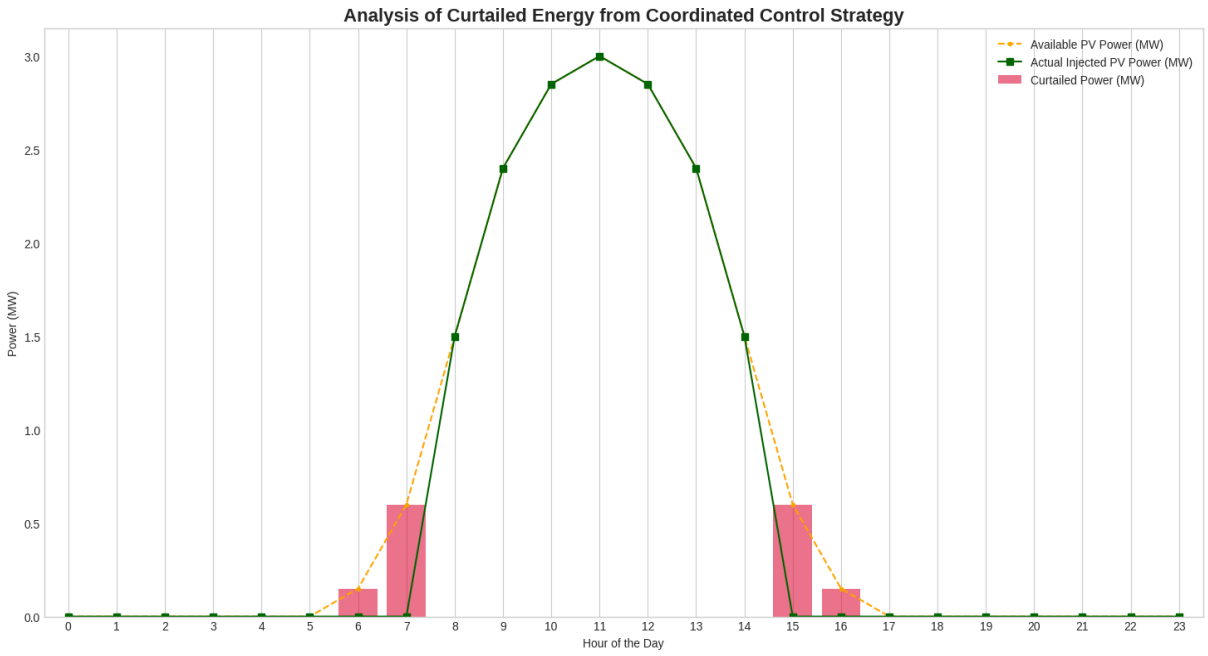

Figure 10 Analysis of energy curtailed by the coordinated control strategy to ensure grid safety

This curtailment occurs during periods of high solar irradiance and low load demand when the PV generation capability significantly exceeds the local consumption. The total curtailed energy ($E_{curtailed}$) was quantified using the relationship previously established in equation (4).

This quantification provides a crucial metric for decision-makers. It highlights a fundamental trade-off: improved grid safety and compliance (achieved through RPF mitigation and voltage stability) come at the cost of a certain amount of forgone renewable energy yield. Understanding this trade-off is vital for optimizing PV integration strategies, encouraging the exploration of complementary solutions such as energy storage or demand-side management to utilize curtailed energy in the future (Rajendran et al., 2025)). The results underscore the necessity of finding the optimal balance point where grid operational integrity is maintained with minimal impact on renewable energy harvesting.

Importantly, the seasonal analysis reveals that this curtailment cost is not uniform throughout the year. The ~1,500 kWh/day curtailment is representative of worst-case dry season conditions. During the rainy season (long rains), the adaptive control imposes effectively zero curtailment, as PV generation naturally remains below the levels that trigger control activation. Assuming approximately 150 dry season days and 100 transition days (with partial curtailment estimated at ~750 kWh/day) per year, the estimated total annual curtailment is approximately 300,000 kWh - substantially less than the 547,500 kWh that would be estimated by extrapolating the dry season curtailment across all 365 days. This more nuanced, seasonally-informed estimate provides a more realistic basis for economic assessments of PV integration under the proposed control strategy.

5. Conclusions

This study thoroughly investigated the critical challenges posed by high photovoltaic (PV) penetration in rural distribution feeders and proposed an adaptive smart inverter control strategy to mitigate these issues. Through comprehensive quasi-static time-series (QSTS) simulations on a validated OpenDSS model of a representative 69 km, 11kV rural feeder in Kenya, this research successfully addressed its stated objectives and research questions.

The initial modelling and analysis confirmed that a significant generation-load mismatch, arising from the cumulative impact of three 1 MW PV systems operating under conventional Maximum Power Point Tracking (MPPT), resulted in severe reverse power flow (RPF) of up to 0.93 MW back into the substation during midday. This condition was identified as a direct threat to grid stability and protection coordination, particularly for rural networks characterized by their high Resistance-to-Reactance (R/X) ratios.

A crucial finding of this research was the diagnosis of the feeder's inherent electrical stiffness. Despite substantial RPF, local voltages at PV connection points did not rise sufficiently (peaking at only 1.038 p.u.) to trigger generic, high-voltage-threshold Volt-Watt curtailment functions.

A key contribution to this study is the comparative seasonal analysis. Rainy season simulations confirmed that RPF does not occur during reduced-irradiance periods, as PV generation (~55-65% of dry season peak) remained below local demand. This establishes RPF as a seasonally bounded challenge. The adaptive control exhibited inherent seasonal intelligence, remaining inactive during the rainy season with zero curtailment, thereby preserving renewable energy yield during low-irradiance months.

The proposed load-following control demonstrated high effectiveness, successfully mitigating the peak RPF by 62.3%, reducing it from 0.93 MW to 0.35 MW. Concurrently, the strategy ensured robust voltage stability, maintaining all nodal voltages within statutory limits (e.g., ±5% of nominal voltage, as per IEEE Std 1547, 2018) throughout the 24-hour simulation period, a significant improvement over uncontrolled MPPT operation.

Finally, the study quantified the economic and operational trade-off associated with achieving grid compliance. The load-matching technique resulted in the curtailment of approximately 1,500 kWh of

renewable energy per day. This quantification provides critical data for stakeholders, highlighting the balance required between maintaining grid integrity and maximizing clean energy yield in high-penetration scenarios. This work validates a practical, context-specific methodology for integrating high levels of PV into challenging rural distribution networks. It emphasizes that tailored, adaptive control strategies are indispensable, moving beyond generic solutions to achieve reliable and safe grid operation. Future research should focus on optimizing the trade-off by exploring advanced forecasting techniques, battery energy storage systems, or demand-side management to utilize curtailed energy, further enhancing the overall economic and environmental benefits of PV integration in rural settings.

Declaration of Ethical Standards

As the authors of this study, we declare that we comply with all ethical standards.

Credit Authorship Contribution Statement

Naomi Muthoni Kamunya: Conceptualization, Methodology, Software (OpenDSS), Data Curation, Investigation, Formal Analysis, Writing _ Original Draft, Visualization, Writing – Review & Editing.
Christopher Maina: Supervision, Conceptualization, Methodology, Writing – Review & Editing.
David Kimemia: Resources, Validation, Project Administration, Writing – Review & Editing.

Declaration of Competing Interest

The authors declared that they have no conflict of interest.

Funding / Acknowledgements

The authors declare that this research received no specific grant from any funding agency in the public, commercial, or not-for-profit sectors.
The authors declare that generative AI was used only for language editing and not for scientific content generation.

Data Availability

The Data that support the findings of this study are available from the Authors upon reasonable request.

References

Azzopardi, B., Gabdullin, Y., & Simkoniene, G. (2023). Photovoltaics and electrical vehicles mitigation on the low-voltage distribution network in Malta. IET Conference Proceedings, 2022(25), 554–556. https://doi.org/10.1049/icp.2023.0053.

Bhatt, P. K. (2022). Solar Energy Integration and Potential Challenges in Distribution Network: A Comprehensive Review. Journal of Energy Research and Reviews, 42–65.

De-Jesús-Grullón, R. E., Batista Jorge, R. O., Espinal Serrata, A., Bueno Díaz, J. E., Pichardo Estévez, J. J., & Guerrero-Rodríguez, N. F. (2024). Modeling and Simulation of Distribution Networks with High Renewable Penetration in Open-Source Software: QGIS and OpenDSS. Energies, 17(12), 2925. https://doi.org/10.3390/en17122925.

Hernández-Mayoral, E., Madrigal-Martínez, M., Mina-Antonio, J. D., Iracheta-Cortez, R., Enríquez-Santiago, J. A., Rodríguez-Rivera, O., Martínez-Reyes, G., & Mendoza-Santos, E. (2023). A Comprehensive Review on Power-Quality Issues, Optimization Techniques, and Control Strategies of Microgrid Based on Renewable Energy Sources. Sustainability, 15(12), 9847. https://doi.org/10.3390/su15129847.

Kariuki, B. W., & Sato, T. (2018). Interannual and spatial variability of solar radiation energy potential in Kenya using Meteosat satellite. Renewable Energy, 116, 88-96. https://doi.org/10.1016/j.renene.2017.09.069.

Khan, H. A., & Rihan, M. (2022). Voltage Regulation Challenges in Highly Solar PV Penetrated Distribution Networks. 2022 1st International Conference on Sustainable Technology for Power and Energy Systems (STPES), 1–6. https://doi.org/10.1109/stpes54845.2022.10006622.

Khatib, T., & Sabri, L. (2021). Grid Impact Assessment of Centralized and Decentralized Photovoltaic-Based Distribution Generation: A Case Study of Power Distribution Network with High Renewable Energy Penetration. Mathematical Problems in Engineering, 2021, 1–16. https://doi.org/10.1155/2021/5430089.

Mehrez, S., Morgan, M., & El Sobki, M. S. (2023). Over Voltage Mitigation in Distribution Systems with High PV Penetration. 2023 24th International Middle East Power System Conference (MEPCON), 1–7. https://doi.org/10.1109/MEPCON58725.2023.10462377.

Mohanty, S., Tripathy, S., Ghatak, S. R., & Mohapatra, A. (2022). Impact Assessment of PV Penetration on Unbalanced Distribution network with Dynamic load condition. 2022 2nd International Conference on Power Electronics & IoT Applications in Renewable Energy and Its Control (PARC), 1–6. https://doi.org/10.1109/PARC52418.2022.9726552.

Okemo, A., Muriithi, C. M., & Nderu, J. (2026). Automated Conversion of Unstructured Geospatial Feeder Data into Analytical Models: An 11 kV Case Study. Electrical Engineering and Energy (ELENE), 1. https://doi.org/10.64470/elene.2026.20.

Pato, P. A. V., Trindade, F. C. L., & Wang, X. (2023). Hosting high PV penetration on distribution feeders with smart inverters providing local var compensation. Electric Power Systems Research, 217, 109168. https://doi.org/10.1016/j.epsr.2023.109168.

Rajendran, G., Raute, R., & Caruana, C. (2025). A Comprehensive Review of Solar PV Integration with Smart-Grids: Challenges, Standards, and Grid Codes. Energies, 18(9), 2221. https://doi.org/10.3390/en18092221

Sharma, V., Haque, M. H., Aziz, S. M., & Kauschke, T. (2023). Smart inverter and battery storage controls to reduce financial loss due to overvoltage-induced PV curtailment in distribution feeders. Sustainable Energy, Grids and Networks, 34, 101030. https://doi.org/10.1016/j.segan.2023.101030.

Wadie, F. (2023). Analysis of the Integrated Effect of Temporary Overvoltages, PV Transformer Connection and Overcurrent Protection in Hybrid PV-Wind Energy System. Electric Power Systems Research, 216, 109084. https://doi.org/10.1016/j.epsr.2022.109084.

Wu, J., Yuan, J., Weng, Y., & Ayyanar, R. (2023). Spatial-Temporal Deep Learning for Hosting Capacity Analysis in Distribution Grids. IEEE Transactions on Smart Grid, 14(1), 354–364. https://doi.org/10.1109/tsg.2022.3196943

Wu, M., Hong, L., Wang, Y., Yan, Z., & Chen, Z. (2022). Volt-VAR control for distribution networks with high penetration of DGs: An overview. The Electricity Journal, 35(5), 107130. https://doi.org/10.1016/j.tej.2022.107130.

Xu, R., Zhang, C., Xu, Y., Dong, Z., & Zhang, R. (2022). Multi-Objective Hierarchically-Coordinated Volt/Var Control for Active Distribution Networks with Droop-Controlled PV Inverters. IEEE Transactions on Smart Grid, 13(2), 998–1011. https://doi.org/10.1109/TSG.2021.3126761.